Large-Area and High-Quality Epitaxial Graphene on Off-Axis SiC Wafers

Abdelkarim Ouerghi,[†,*] Mathieu G. Silly,[‡] Massimiliano Marangolo,[§] Claire Mathieu,[†] Mahmoud Eddrief,[§] Matthieu Picher,[†] Fausto Sirotti,[‡] Souliman El Moussaoui,[‡] and Rachid Belkhou[‡]

[†]Laboratoire de Photonique et de Nanostructures (CNRS-LPN), Route de Nozay, 91460 Marcoussis, France, [‡]Synchrotron-SOLEIL, Saint-Aubin, BP48, F91192 Gif sur Yvette Cedex, France, and [§]Institut des NanoSciences de Paris, UPMC—CNRS, UMR 7588, 4 Place Jussieu, 75005 Paris, France

ABSTRACT

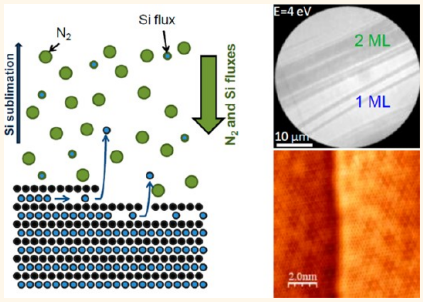

The growth of large and uniform graphene layers remains very challenging to this day due to the close correlation between the electronic and transport properties and the layer morphology. Here, we report the synthesis of uniform large-scale mono- and bilayers of graphene on off-axis 6H-SiC(0001) substrates. The originality of our approach consists of the fine control of the growth mode of the graphene by precise control of the Si sublimation rate. Moreover, we take advantage of the presence of nanofacets on the off-axis substrate to grow a large and uniform graphene with good long-range order. We believe that our approach represents a significant step toward the scalable synthesis of graphene films with high structural qualities and fine thickness control, in order to develop graphene-based electronic devices.

KEYWORDS: epitaxial graphene · spectroscopy · vicinal SiC · scanning tunneling microscopy · low-energy electron microscopy · electronic properties

The recent discovery of the electronic properties of a graphene layer[1−3] has fostered the exciting research field of graphene-based materials, in turn stimulating many new discoveries[4] and potential applications.[2] Graphene is a zero band gap material with very unique electronic and optical properties including extremely high carrier mobility, massless Dirac fermions, and quantum Hall effects at room temperature.[3] This has led to a tremendous rise in experimental research on graphene for applications such as ultra-high-speed field-effect transistors, p−n junction diodes, terahertz oscillators, optical sensors, and low-noise electronics.[4,5] Up to now, a large number of fundamental studies of graphene have been carried out using micromechanical cleavage of single-layer flakes from graphite,[2] chemical vapor deposition (CVD) of carbon on single-crystal transition metals,[6,7] or epitaxial growth by thermal decomposition of SiC surfaces.[1] The two latter approaches have already been shown to reach large-scale graphene.

For electronic applications, the epitaxial growth of graphene by CVD presents a drawback since it requires transferring the graphene onto an insulating substrate. This transfer step involves heavy chemical manipulation and can result in contamination and limiting of the mobility of the sample. In the case of epitaxial graphene on SiC, the substrate acts already as an insulator, so that intrinsic properties of graphene are preserved. Moreover epitaxial graphene on SiC is suitable for optics, because the substrate is transparent over a very broad frequency spectrum, and for application in high-frequency devices, where losses due to residual conductivity of the substrate have to be minimized by using high-quality insulating materials. Nevertheless, control of the preparation conditions for homogeneous large-area graphene layers remains a challenge. Indeed, on the on-axis Si-terminated SiC substrate, vacuum annealing leads only to small graphene domains (a few hundred nanometers) with nonuniform multilayers growing simultaneously.[4,8] It appears that this limitation is mainly due to the high sublimation rate of Si atoms from SiC substrates at elevated temperatures (~1400 °C). Therefore, homogeneity can be significantly improved by a better control of the sublimation rate of Si atoms (Figure 1). Recent approaches have been taken toward higher-quality films involving heating under argon at atmospheric pressure[8,9] or supplying an excess of Si in the gas phase.[10] These new approaches enable significant improvements in domain size and in the electronic properties compared to vacuum

* Address correspondence to Abdelkarim.Ouerghi@lpn.cnrs.fr.

Received for review March 15, 2012 and accepted June 16, 2012.

Published online June 17, 2012
10.1021/nn301152p

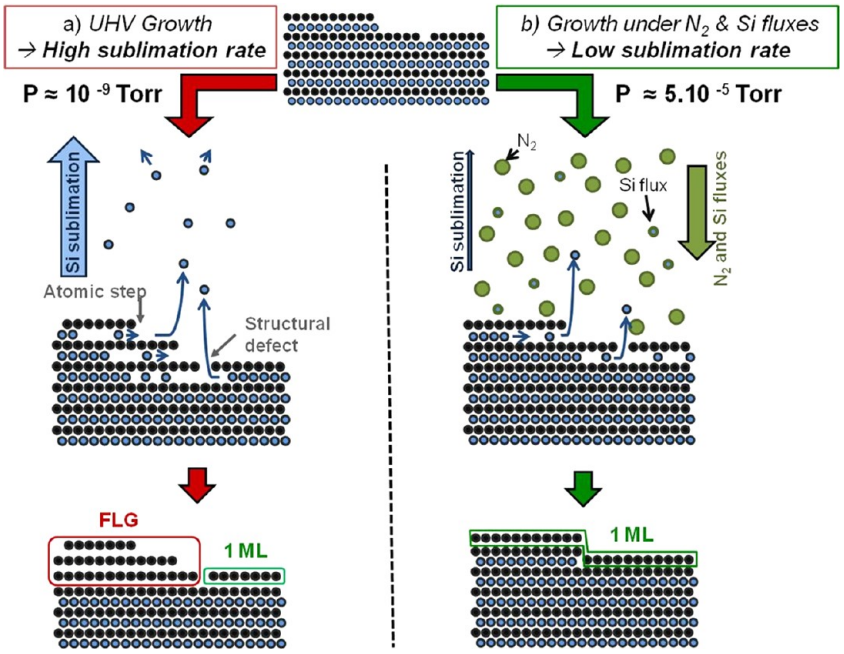

Figure 1. (a) Epitaxial graphene grown under UHV conditions explaining the formation of different thicknesses over the surface. (b) Epitaxial graphene growth under N_2 and Si fluxes, generating a uniform graphene monolayer.

graphitization.[8] However, the on-axis SiC presents a large number of step bunching effects,[11−13] which remains a severe limitation to producing high-quality graphene layers. Indeed the height of these steps can prevent the formation of a continuous graphene layer between two adjacent terraces. Moreover, it has recently been demonstrated that even for continuous layers the SiC step edge can affect the electronic properties of epitaxial graphene, reducing the mobility.[14] On the other side, on the off-axis SiC substrate the presence of step bunching is highly reduced, as it preferentially forms nanofacets instead of steps. Furthermore, the H_2 etching before the graphene growth and the N_2 flux can be used during the graphitization to favor the formation of these nanofacets. This would facilitate the reduction of the number of steps of the SiC substrate and therefore generate a homogeneous graphene layer over the whole sample.

We demonstrate here the successful growth of ordered graphene layers on off-axis SiC substrates up to an unprecedentedly large dimension up to hundreds of micrometers, by combining N_2 and Si fluxes during the graphitization. The graphene layer is formed on the off-axis SiC without modification of the original surface morphology. The high crystallinity of the graphene layers and the two-dimensional hexagonal arrangement of carbon atoms were further confirmed by high-resolution scanning tunneling microscopy (STM), low-energy electron microscopy (LEEM), low-energy electron diffraction (LEED), and micro-Raman spectroscopy. X-ray photoelectron (XPS) and angle resolved photoemission spectroscopy (ARPES) were used to describe the electronic properties of the graphene layer. Our results confirm that the extremely high temperature annealing process used in combination with an N_2 and Si flux is the key factor in generating large homogeneous graphene layers on off-axis SiC. These observations can be of prime importance, in particular in view of developing graphene-based electronic devices.

RESULTS AND DISCUSSION

Epitaxial graphene was produced on a semi-insulating off-axis SiC(0001) substrate with periodic nanofacets[15] (Si-face, 3.5° off toward [11−20]). During the graphene growth process, the samples were exposed to a N_2 partial pressure of $P = 2 \times 10^{-5}$ Torr and Si deposition rate of 1 ML/min. Figure 2 shows typical LEEM images at different stages of epitaxial graphene: (a−c) formation of the first layer between 1200−1300 °C, (d) growth of the second-layer at 1350 °C. The LEEM image (Figure 2a) displays the beginning of graphene formation. Some sharp dark lines, which are all aligned along the ⟨1−100⟩ SiC axis, start to appear on the surface (blue arrow), showing that the first layer nucleates on the interterrace nanofacets.[5,15] These lines appear longer and wider when the annealing temperature is increased (Figure 2b), demonstrating that graphene propagates laterally along the nanofacets. Typically these ribbons are 5 μm wide and ~500 μm long and are all aligned along the ⟨1−100⟩ SiC axis, as it has already been observed on the SiC-(000−1) surface.[16,17] It is worthwhile noting that some of these ribbons are much wider than the underlying step distances on the off-axis substrate (500 nm), suggesting that the graphene then expands on the terraces

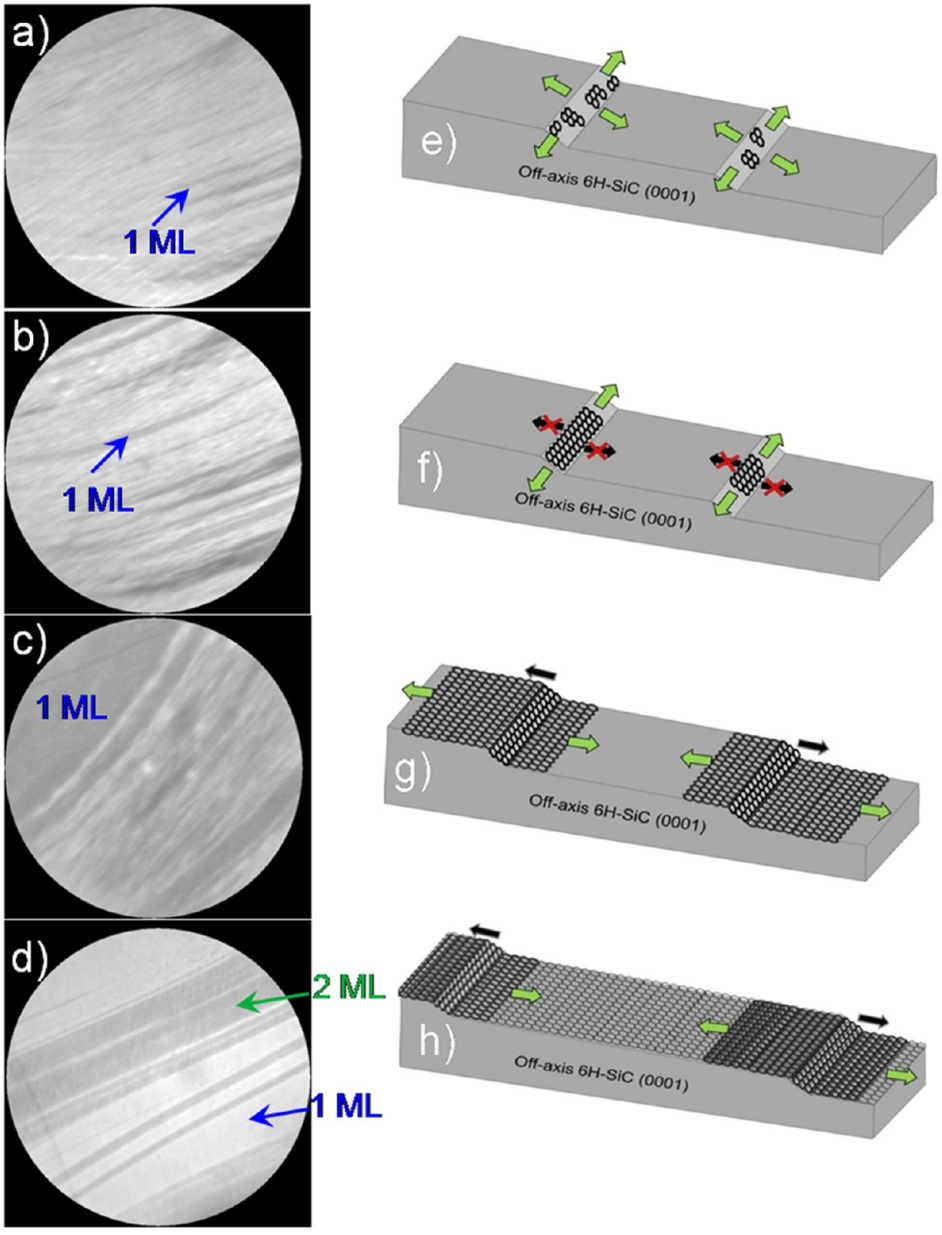

Figure 2. (a–d) LEEM images taken at different annealing temperature: (a) 1200 °C, (b) 1250 °C, (c) 1300 °C, and (d) 1350 °C. The contrast represents different layers: for images (a) to (c) the bright (dark, respectively) contrast corresponds to the substrate (1 ML), and for image (d) the bright and dark contrasts are associated with 1 and 2 ML substrate, respectively. The primary electron energy used is $E_{vac} = +4.0$ eV, and the field of view was set to 50 μm. (e–h) Schematic steps of the graphene growth: the graphene starts to grow in the vicinity of nanofacet regions (e). Carbon atoms then diffuse and nucleate parallel to the step edges (f). The ribbons propagate laterally toward the center of the terraces (g). A second graphene layer start to grow on the same nucleation sites (h).

and at the end coalesces very uniformly over the whole surface in the limit of LEEM resolution. However, we do not currently exclude the formation of the domain boundary at low scale resulting from the coalescence of different graphene ribbons. The graphene expansion is confirmed in Figure 2c, which displays large graphene monolayers, suggesting that the domains are partially unified without secondary nucleation events (layer-by-layer growth mode). Therefore, one can easily understand that the number of nucleation sites depends strongly on the number of nanofacets generated on off-axis SiC substrates. Figure 2c also shows graphene domains whose sizes exceed the average step spacing on the SiC substrate by about 2 orders of magnitude. This observation demonstrates a continuous, carpet-like flow of the graphene sheet across substrate steps.[6,18]

The second layer of graphene starts to grow at above 1350 °C (Figure 2d), as shown by the darker fine ribbons covering about half of the surface area (green arrows) on this area. This observation suggests that the formation of the second graphene layer follows

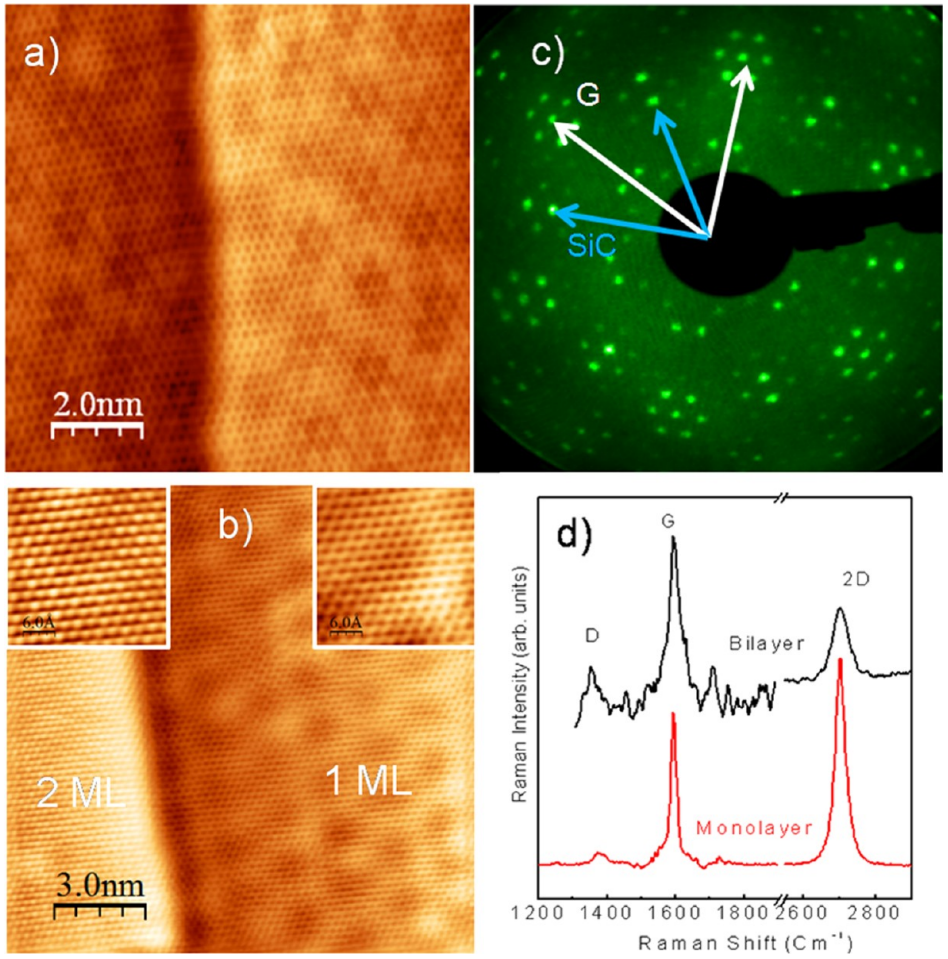

Figure 3. (a) STM image of a graphene monolayer on 6H-SiC(0001). A honeycomb-type structures on the step edges of SiC substrate can be observed, demonstrating the continuity of the layer (−0.05 mV, 0.1 nA) (b) STM image of the interface between the graphene bilayer and monolayer regions (V = 50 meV, I = 500 pA). The left inset in (b) clearly reveals a honeycomb array, while the right inset presents a triangular lattice of graphene monolayer and bilayer (V = 50 meV, I = 500 pA). (c) LEED pattern of epitaxial graphene annealed at 1350 °C (electron energy: 98 eV). (d) Micro-Raman spectra of the D, G, and 2D bands for the graphene monolayer and bilayer.

the same template as the first one. Robinson *et al.* observed that graphene growth happens mainly on nanofacets leading to multilayers.[19] However, this is clearly not the case here: the process of graphene formation on an off-axis SiC(0001) substrate can be summarized in the diagram presented in Figure 2e−h. We suggest that the graphene starts to grow in the vicinity of nanofacet regions consisting of step edges (Figure 2e). These preferential nucleation sites can be explained by the fact that the Si atoms in the nanofacets present a higher number of dangling bonds[5] relative to the Si atoms of the terraces, which confer on them a higher reactivity and a low cohesive energy. These nucleation sites are one of the key factors that govern the formation of large domains. Carbon atoms then diffuse and nucleate parallel to the step edges (Figure 2f). The C diffusion perpendicular to the step edges toward the terrace regions may initially be energetically less favorable, resulting in a high ribbon density. Nevertheless, at higher annealing temperatures, these ribbons coalesce and gradually propagate laterally toward the center of the terraces (Figure 2g), before generating a second graphene layer (Figure 2h). This growth process forms a large area and a smooth layer due to a carpet-like behavior, which drapes the edges without interruption, highlighting the possibility of growing large-scale graphene on off-axis SiC.[12,13,20]

Below, only the results obtained on the sample annealed up to 1350 °C will be presented, as these are representative of the desired uniform monolayer, on which few bilayer ribbons of graphene had started to grow. For the following experiments, the bilayer coverage was estimated to be around 15%. In order to understand which type of carbon overlayer was actually formed (graphite, graphene, or both), LEED, STM, and Raman spectroscopy were used, as shown in Figure 3. The crystalline continuity of the graphene over steps is supported by STM images. Figure 3a and b present typical STM images of the sample. Figure 3a shows a graphene monolayer over a step edge with an atomic resolution. The honeycomb lattice structure is resolved on both upper and lower terraces with

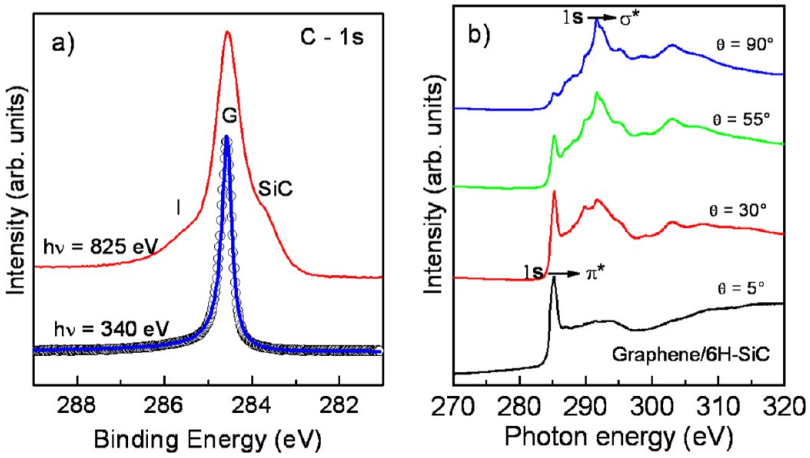

Figure 4. (a) C 1s XPS spectra for epitaxial graphene annealed at 1350 °C at $h\nu$ = 340 eV (bottom) and $h\nu$ = 825 eV (top). XPS measurements were performed at φ = 70° emergency angle with respect to the sample normal. The bottom spectrum was fitted using a Doniach−Sunjic line-shape analysis. (b) Carbon K-edge NEXAFS spectra of this sample, measured for various angles of incidence of X-rays. The features at 285.2 and 291.5 eV are attributed to the 1s→π* and 1s→σ* transitions, respectively.

the lattice orientation remaining unchanged. Moreover the honeycomb lattice structure of the graphene overlayer remains perfect over the step, which further demonstrates that the graphene is continuous over the step edge. An atomically resolved STM image of the interface between the bilayer regions and the monolayer graphene on a (0001) terrace is shown in Figure 3b. This image shows the coexistence of two regions with a 0.3 nm height difference. The step delineates the domain boundary separating these two regions. This image shows a continuous top layer graphene on the steps edge. An atomically resolved STM image of the left region is shown as an inset (left inset in Figure 3b), clearly revealing a honeycomb array, characteristic of a graphene monolayer. The stacking-induced asymmetry is absent, and consequently all atomic sites are equivalent. Long-range periodicity in charge density from the underlying well-known (6×6) reconstructed interface layer was typically observed over a 10 × 10 nm^2 scan area.[21] The right inset image presents a triangular lattice, indicating that only one of the two graphene sublattices is imaged due to Bernal stacking of a graphene bilayer. Similar images have been observed in STM studies of bulk graphite and multilayer graphene surfaces.[22] The LEED pattern (Figure 3c) includes two contributions. The first arises from the sharp (1×1) graphene layer and confirms the presence of a homogeneous surface. The second one, which is characterized by isotropic (circular) 1/6 fractional spots, is attributed to the $(6\sqrt{3}\times6\sqrt{3})R30°$ reconstructed layer. We can, without any doubt, conclude that the graphene monolayer exhibited a high crystalline quality and a uniform in-plane orientation with respect to the average normal to the substrate surface.

We also used micro-Raman spectroscopy to probe the consequences of the presence of microsized ribbons on the vibrational and electronic properties of graphene on an off-axis SiC substrate. Figure 3d shows two representative Raman spectra of a graphene/SiC system in the wavelength range 1200−3000 cm^{-1}.[23] Numerous spectra were acquired in different areas of the substrate in order to check the uniformity of the signal. This signal exhibits the three main peaks expected for graphene samples: (i) D band at 1355 cm^{-1}, (ii) G band at 1595 cm^{-1}, and (iii) 2D band at 2705 cm^{-1}. The intensity ratio of the defect-induced D band to the graphite G band has been widely used to estimate the density of defects in graphene.[24] In our case, the high G over D ratio demonstrates the good structural quality of the grown graphene. Moreover, the 2D band was observed at 2705 cm^{-1} with a full width half-maximum of 32 and 53 cm^{-1}, indicating the presence of a monolayer and bilayer. The G and 2D bands were observed at 1595 and 2705 cm^{-1}, respectively, which was higher than those expected for graphene made by micromechanical cleavage.[25] This shift toward higher wavelengths could be due to doping or strain effects. However, it is well known that the Raman blue shift due to doping is more important for the G band than for the 2D band.[25,26] Therefore, the shift of the G band was too small compared to that measured on the 2D band to be attributed to electron or hole doping effects. We can safely conclude that this blue-shift can be explained only by a low compressive strain of the graphene lattice. The origin of this strain in epitaxial graphene is usually attributed to the large difference in the in-plane thermal expansion coefficient between the SiC and the graphene layer. From the 2D Raman peak, we estimate the compressive strain at 0.07%, and it has been deduced according to the work of Ferralis *et al.*[23] This low strain can be explained by the morphology of the off-axis surface and the carpet-like growth mode, which facilitates relaxation due to the nanofacets of the step edge geometry.

We probed the electronic properties of the sample annealed at 1350 °C further using photoelectron spectroscopy and near-edge X-ray absorption fine structure (NEXAFS) experiments (Figure 4). The C 1s XPS spectrum of this sample, collected for $h\nu = 340$ eV, is shown in Figure 4a. Due to the low electron inelastic mean free path at this photon energy, only the first 1−3 topmost layers are probed. A sharp C 1s peak, labeled G, located at 284.5 eV in binding energy, indicates the presence of sp^2-hybridized C−C bonds. The spectrum was further fitted using a Doniach−Sunjic line shape with an asymmetry factor α of 0.08 and a fwhm of 0.125 eV. The very low value of the fwhm indicates that only one core level peak was present and thus that the carbon atoms had a unique chemical environment. At higher photon energy ($h\nu$ = 825 eV), the C 1s spectrum showed three components at 283.4, 284.4, and 284.9 eV in binding energy (Figure 4a). These components correspond to the SiC bulk (noted SiC), the graphene layer (noted G), and the interface layer (noted I), respectively. The presence of a unique peak for $h\nu$ = 340 eV (surface sensitive) and three components for $h\nu$ = 825 eV (bulk sensitive) confirmed the monolayer and/or bilayer nature of the graphene.[8,9,21,27] Moreover, no structure appeared at ~286.7 in C-1s XPS spectra, usually attributed to the presence of COOH groups, as a result of contamination and/or oxidation; this means that even if the samples were prepared under high-pressure conditions ($P = 2 \times 10^{-5}$ Torr), the graphene layers were very inert and did not show any contamination in this moderate vacuum. Unoccupied electronic states of graphene were examined by NEXAFS spectroscopy. Figure 4b shows the C 1s NEXAFS spectra measured for different incidence angles of the linearly polarized synchrotron light. In this geometry, the horizontally linear polarized light was almost parallel to the sample normal at grazing incidence and lay within the sample plane in normal incidence geometry. In these spectra two kinds of resonance could be observed at photon energies of 285.2 and 291.5 eV: these two peaks were characteristic of graphene on SiC.[28] The first transition, a very sharp feature at 285.4 eV with a maximum intensity at $\theta = 0°$, arises from an excitation into the antibonding π*-band in the region of the M point of the Brillouin zone. The second, appearing at 291.8 eV with maximum intensity at $\theta = 90°$, is attributed to an excitation in the antibonding σ*-band. Recently, it was shown that C 1s NEXAFS spectral line shapes may be strongly affected by interaction between the graphene layer and the substrate. As no other significant features, apart from the σ* and π* transitions, could be observed on these NEXAFS spectra, the graphene layers presented a high degree of crystallinity and were uniformly parallel to the substrate surface. In our sample, the disorientation of the nanofacets did not seem to affect the σ* and π* transitions, characteristic of graphene on SiC.[28]

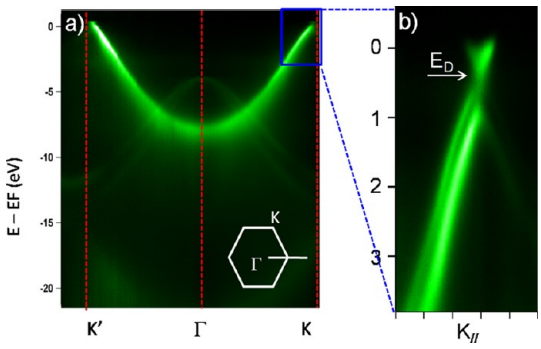

Figure 5. (a) 2D band structure map along the K′ΓK direction, obtained by ARPES ($h\nu$ = 50 eV) at room temperature, on epitaxial graphene annealed at 1350 °C. Inset of (a) shows the Brillouin zone of graphene, and the horizontal line in the KM direction presents the measurement geometry in *k*-space. (b) Zoom-in of the band structure around the K point. The Dirac point, indicated by the white arrow, is pushed by 0.3 eV below the Fermi level.

However, the faint features observed around the σ* transition could be due to facet disorientation.

The electronic structure was also probed using angle-resolved photoemission spectroscopy, which is a powerful method for this purpose, as it gives direct access to the spectral function containing the information on electron energy band dispersion. The measured ARPES band structure map is displayed in Figure 5, in which the photoelectron intensity is presented as a function of energy and *k*-momentum, along the K′−Γ−K direction of the first Brillouin zone. It is obvious that the sharp and intense structure of the two π-bands confirms the high structural quality of the graphene layer.[29,30] Close inspection of the dispersion relation around the K point reveals that, similar to graphene on on-axis 6H-SiC, the Dirac point (E_D) is pushed by 0.3 eV below the Fermi level. This is what is usually expected from a pure graphene layer on SiC, as the substrate and the interface layer act as dopant for the graphene layer. The linearity of the π-band around the K point is characteristic of a signature of massless Dirac fermions. The electron doping level can be estimated at about 6.6×10^{12} cm^{-2}. Furthermore, the π-band splits into two bands, due to an interlayer decoupling, proving that a graphene bilayer is also present at the surface, which is consistent with the LEEM observation (Figure 2d). To evaluate the electronic quality of our graphene layers, we determined the carrier mobility of the sample using van der Pauw measurements at room temperature. The electron density in several areas of this sample was typically 6×10^{12} cm^{-2}, with a macroscopically averaged electron mobility inferred from Hall voltage estimated at about 1700 $cm^2/(V\ s)$.

From the data presented in Figures 2 and 3, it is clear that graphene grows in size up to a large scale and presents a good long-range order. Hereafter, the origin of this growth improvement is discussed. The results of

our SiC substrates evaporation experiments are as follows: (a) the major vapor species are Si and C; (b) below the temperature T_C SiC evaporates congruently, whereas above T_C silicon is preferentially lost; (c) the T_C value varies with the crystallographic orientation and is higher for the (0001) terraces and lower for the (1−10*n*) nanofacets. The rate of free Si evaporation is proportional to the equilibrium partial pressure of the respective species based on the Langmuir equation. In our case, the decomposition of SiC was controlled by (and was equal to) the evaporation of Si atoms. This is why we used N_2 and Si fluxes during the sublimation growth experiments in order to reduce a too fast sublimation rate and to provide a smooth decomposition of the SiC.

A highly interesting aspect of our growth method was the continuity of the graphene lattice over the regularly stepped 6H-SiC. This structure is of particular interest because the stepped surface is expected to produce a periodic strain that is strictly mechanical in nature, as well as a charge modulation beneath the graphene. This modulation is a result of confinement, with a significant one-dimensional (1D) or two-dimensional (2D) lateral potential modulation induced by the nanofacet of the 6H-SiC substrate. These effects have been exploited to induce measurable band gaps in graphene's electronic structure with the hope of making practical carbon-based logic devices.[5,31] Another attractive aspect is the presence of auto-organized ribbons, generated at the early stage of the first layer growth. Ribbons with such widths are expected to be semiconductors with a band gap inversely proportional to the width.[32] This observation seems to be very promising for microelectronic applications using the 1D structure of carbon. Indeed, the appearance of ferromagnetism was recently theoretically suggested because of localized spins around the elbows of the zigzag, which give a strong exchange interaction.[33] On the other hand, other theoretical calculations predict a localized metallic state for the zigzag edge.[34]

CONCLUSIONS

In summary, we have developed a new method for synthesizing large-scale graphene on an off-axis 6H-SiC-(0001) substrate. This graphene exhibits a remarkable continuity on terraces and over step edges, suggesting the possibility of growing large-scale graphene layers with high long-range order. In particular, the micro-Raman spectroscopy showed the presence of monolayer and bilayer graphene. The LEEM data show that a uniform monolayer can be observed over the whole sample with a small amount of bilayers (∼15%), while the ARPES data suggest that graphene is electron doped. Our STM results demonstrate that the growth of graphene is continuous over the step edges. It may be possible to exploit such substrates for periodic charge modulation, as well as atomic lattice registry for postmodification studies. Altogether, these findings open a new route to obtaining uniform high-quality wafer size graphene layers for future electronic device applications.

METHODS

The substrates used in these studies were semi-insulating off-axis SiC(0001) (Si-face, 3.5° off toward [11−20][12,13]). The samples were further exposed to hydrogen etching at 1600 °C in order to remove polishing damage and residual oxides. This step of the sample preparation gives the SiC surface a self-ordered surface structure consisting of pairs of 280 nm wide (0001) terraces and 30 nm wide (1−10*n*) nanofacets.[15] During the graphene growth process, the samples were exposed to a N_2 partial pressure of $P = 2 \times 10^{-5}$ Torr and Si deposition rate of 1 ML/min, while the substrate was annealed at a temperature range of 1200−1350 °C. This induced a growth of (3×3), $(\sqrt{3}\times\sqrt{3})R30°$, and $(6\sqrt{3}\times6\sqrt{3})R30°$ reconstructions as intermediate steps. Moreover, introducing N_2 gas decreases the growth rate and energetically stabilizes the nanofacet surfaces during epitaxial graphene growth. The samples were then cooled to room temperature and transferred *ex situ* from the growth chamber to undergo LEEM, STM, XPS, and ARPES measurements. Before each measurement, samples were annealed at 600 °C for 30 min to remove surface contaminations. Sample cleanness was checked each time using Auger spectroscopy.

LEEM measurements at room temperature (Elmitec GmBH−LEEM III) with a spatial resolution better than 30 nm were carried out at the CEA/IRAMIS/SPCSI laboratory (Saclay, France). The bias difference between the electron gun and sample was the start voltage and was roughly equal to the primary electron beam energy.

STM experiments were carried out using an UHV AFM-STM Omicron at room temperature.

The micro-Raman spectroscopy was performed at room temperature with a Renishaw spectrometer using 514 nm laser light focused on the sample by a DMLM Leica microscope with a 50× (NA = 0.75) objective and a power of 5 mW with a spot size of about 1 μm.

XPS, NEXAFS, and ARPES measurements were performed on the TEMPO beamline of the SOLEIL synchrotron (Saint-Aubin, France). The analyzing chamber was equipped with a SCIENTA-2000 electron hemispherical analyzer with a delay-line 2D detector, which optimized the detection linearity and signal/background ratio. XPS measurements were performed at grazing emergency of the photoelectron, which is the same experimental geometry used to study the states at the Fermi level. The Dirac cones were imaged at 25° with respect to the normal surface. The C-1s core level was then recorded with a 70° angle of emergence with respect to the sample normal, which increases the surface sensitivity of the measurement.

For ARPES measurements, the photon energy ($h\nu$ = 50 eV) and sample orientation were set in order to explore the *k*-space region around the K point in the ΓK direction of the Brillouin zone. The photon beam impinged on the sample at an angle of 43°, and photoelectrons were detected around the sample surface normal with an angular acceptance of 6°.

Conflict of Interest: The authors declare no competing financial interest.

Acknowledgment. We are grateful to B. Etienne and E. Pallecchi for fruitful discussions and to D. Martinotti for his outstanding work and technical assistance during the LEEM experiments at the CEA/IRAMIS/SPCSI laboratory. This work was supported by the ANR (Migraquel and SUPERTRAMP) grants and the RTRA Triangle de la Physique.

REFERENCES AND NOTES

1. Berger, C.; Song, Z.; Li, T.; Li, X.; Ogbazghi, A. Y.; Feng, R.; Dai, Z.; Marchenkov, A. N.; Conrad, E. H.; First, P. N.; *et al.* Ultrathin Epitaxial Graphite: 2D Electron Gas Properties

and a Route toward Graphene-Based Nanoelectronics. *J. Phys. Chem. B* **2004**, *108*, 19912–19916.
2. Novoselov, K. S.; Geim, A. K.; Morozov, S. V.; Jiang, D.; Katnelson, M. I.; Grigorieva, I. V.; Dubonos, S. V.; Firsov, A. A. Two-Dimensional Gas of Massless Dirac Fermions in Graphene. *Nature* **2005**, *438*, 197–200.
3. Novoselov, K. S.; Jiang, Z.; Zhang, Y.; Morozov, S. V.; Stormer, H. L.; Zeitler, U.; Maan, J. C.; Boebinger, G. S.; Kim, P.; Geim, A. K. Room-Temperature Quantum Hall Effect in Graphene. *Science* **2007**, *315*, 1379–1379.
4. Berger, C.; Song, Z.; Li, X.; Wu, X.; Brown, N.; Naud, C.; Mayou, D.; Li, T.; Hass, J.; Marchenkov, A. N.; *et al*. Electronic Confinement and Coherence in Patterned Epitaxial Graphene. *Science* **2006**, *312*, 1191–1196.
5. Sprinkle, M.; Ruan, M.; Hu, Y.; Hankinson, J.; Rubio-Roy, M.; Zhang, B.; Wu, X.; Berger, C.; de Heer, W. A. Scalable Templated Growth of Graphene Nanoribbons on SiC. *Nat. Nanotechnol.* **2010**, *5*, 727–731.
6. Sutter, P. W.; Flege, J. I.; Sutter, E. A. Epitaxial Graphene on Ruthenium. *Nat. Mater.* **2008**, *7*, 406–411.
7. Balog, R.; Jørgensen, B.; Nilsson, L.; Andersen, M.; Rienks, E.; Bianchi, M.; Fanetti, M.; Lægsgaard, E.; Baraldi, A.; Lizzit, S.; *et al*. Bandgap Opening in Graphene Induced by Patterned Hydrogen Adsorption. *Nat. Mater.* **2010**, *9*, 315–319.
8. Emtsev, K. V.; Bostwick, A.; Horn, K.; Jobst, J.; Kellogg, G. L.; Ley, L.; McChesney, J. L.; Ohta, T.; Reshanov, S. A.; Röhrl, J.; *et al*. Towards Wafer-Size Graphene Layers by Atmospheric Pressure Graphitization of Silicon Carbide. *Nat. Mater.* **2009**, *8*, 203–207.
9. Virojanadara, C.; Syväjarvi, M.; Yakimova, R.; Johansson, L. I.; Zakharov, A. A.; Balasubramanian, T. Homogeneous Large-Area Graphene Layer Growth on 6H-SiC(0001). *Phys. Rev. B* **2008**, *78*, 245403.
10. Tromp, R. M.; Hannon, J. B. Thermodynamics and Kinetics of Graphene Growth on SiC(0001). *Phys. Rev. Lett.* **2009**, *102*, 106104.
11. Seyller, Th.; Emtsev, K. V.; Gao, K.; Speck, F.; Ley, L.; Tadich, A.; Broekman, L.; Riley, J. D.; Leckey, R. C. G.; Rader, O.; *et al*. Structural and Electronic Properties of Graphite Layers Grown on SiC(0001). *Surf. Sci.* **2006**, *600*, 3906–3911.
12. Penuelas, J.; Ouerghi, A.; Lucot, D.; David, C.; Gierak, J.; Estrade-Szwarckopf, H.; Andreazza-Vignolle, C. Surface Morphology and Characterization of Thin Graphene Films on SiC Vicinal Substrate. *Phys. Rev. B* **2009**, *79*, 033408.
13. Tanaka, S.; Morita, K.; Hibino, H. Anisotropic Layer-by-Layer Growth of Graphene on Vicinal SiC(0001) Surfaces. *Phys. Rev. B* **2010**, *81*, 041406.
14. Ji, S.-H.; Hannon, J. B.; Tromp, R. M.; Perebeinos, V.; Tersoff, J.; Ross, F. M. Atomic-Scale Transport in Epitaxial Graphene. *Nat. Mater.* **2012**, *11*, 114–119.
15. Fujii, M.; Tanaka, S. Ordering Distance of Surface Nanofacets on Vicinal 4H-SiC(0001). *Phys. Rev. Lett.* **2007**, *99*, 016102.
16. Camara, N.; Huntzinger, J.-R.; Rius, G.; Tiberj, A.; Mestres, N.; Pérez-Murano, F.; Godignon, P.; Camassel., J. Anisotropic Growth of Long Isolated Graphene Ribbons on the C Face of Graphite-Capped 6H-SiC. *Phys. Rev. B* **2009**, *80*, 125410.
17. Camara, N.; Jouault, B.; Caboni, A.; Jabakhanji, B.; Desrat, W.; Pausas, E.; Consejo, C.; Mestres, N.; Godignon, P.; Camassel, J. Growth of Monolayer Graphene on 8° Off-Axis 4H−SiC (000−1) Substrates with Application to Quantum Transport Devices. *Appl. Phys. Lett.* **2010**, *97*, 093107.
18. Vecchio, C.; Sonde, S.; Bongiorno, C.; Rambach, M.; Yakimova, R.; Raineri, V.; Giannazzo, F. Nanoscale Structural Characterization of Epitaxial Graphene Grown on Off-Axis 4H-SiC (0001). *Nanoscale Res. Lett.* **2011**, *6*, 269.
19. Robinson, J.; Weng, W.; Trumbull, K.; Cavalero, R.; Wetherington, M.; Frantz, E.; LaBella, M.; Hughes, Z.; Fanton, M.; Snyder, D. Nucleation of Epitaxial Graphene on SiC(0001). *ACS Nano* **2010**, *4*, 153–158.
20. Norimatsu, W.; Kusunoki, M. Formation Process of Graphene on SiC(0001). *Phys. E (Amsterdam, Neth.)* **2010**, *42*, 691–694.
21. Ouerghi, A.; Kahouli, A.; Lucot, D.; Portail, M.; Travers, L.; Gierak, J.; Penuelas, J.; Jegou, P.; Shukla, A.; Chassagne, T.; *et al*. Epitaxial Graphene on Cubic SiC(111)/Si(111) Substrate. *Appl. Phys. Lett.* **2010**, *96*, 191910.
22. Mallet, P.; Varchon, F.; Naud, C.; Magaud, L.; Berger, C.; Veuillen, J. Y. Electron States of Mono- and Bilayer Graphene on SiC Probed by Scanning-Tunneling Microscopy. *Phys. Rev. B* **2007**, *76*, 041403.
23. Ferralis, N.; Maboudian, R.; Carraro, C. Evidence of Structural Strain in Epitaxial Graphene Layers on 6H-SiC(0001). *Phys. Rev. Lett.* **2008**, *101*, 156801.
24. Ferrari, A. C. Raman Spectroscopy of Graphene and Graphite: Disorder, Electron−Phonon Coupling, Doping and Nonadiabatic Effects. *Solid State Commun.* **2007**, *143*, 47–57.
25. Das, A.; Pisana, S.; Chakraborty, B.; Piscanec, S.; Saha, S. K.; Waghimare, U. V.; Novoselov, K. S.; Krishnamurthy, H. R.; Geim, A. K.; Ferrari, A. C.; *et al*. Monitoring Dopants by Raman Scattering in an Electrochemically Top-Gated Graphene Transistor. *Nat. Nanotechnol.* **2008**, *3*, 210–215.
26. Ni, Z. H.; Chen, W.; Fan, X. F.; Kuo, J. L.; Yu, T.; Wee, A. T. S.; Shen, Z. X. Raman Spectroscopy of Epitaxial Graphene on a SiC Substrate. *Phys. Rev. B* **2008**, *77*, 115416.
27. Ouerghi, A; Ridene, M; Balan, A; Belkhou, A; Barbier, A; Gogneau, N; Portail, M; Michon, A; Latil, S; Jegou, P.; *et al*. Sharp Interface in Epitaxial Graphene Layers on 3*C*-SiC-(100)/Si(100) Wafers. *Phys. Rev. B* **2011**, *83*, 205429.
28. Aristov, V. Y.; Urbanik, G.; Kummer, K.; Vyalikh, D. V.; Molodtsova, O. V.; Preobrajenski, A. B.; Zakharov, A. A.; Hess, C.; Hanke, T.; Buchner, B.; *et al*. Graphene Synthesis on Cubic SiC/Si Wafers. Perspectives for Mass Production of Graphene-Based Electronic Devices. *Nano Lett.* **2010**, *10*, 992–995.
29. Ohta, T.; Bostwick, A.; Seyller, T.; Horn, K.; Rotenberg, E. Controlling the Electronic Structure of Bilayer Graphene. *Science* **2006**, *313*, 951–954.
30. Ouerghi, A.; Belkhou, R.; Marangolo, M.; Silly, M. G.; El Moussaoui, S.; Eddrief, M.; Largeau, L.; Portail, M.; Sirotti, F. Structural Coherency of Epitaxial Graphene on 3C-SiC-(111) Epilayers on Si(111). *Appl. Phys. Lett.* **2010**, *97*, 161905.
31. Odaka, S.; Miyazaki, H.; Li, S.-L.; Kanda, A.; Morita, K.; Tanaka, S.; Miyata, Y.; Kataura, H.; Tsukagoshi, K.; Aoyagi, Y. Anisotropic Transport in Graphene on SiC Substrate with Periodic Nanofacets. *Appl. Phys. Lett.* **2010**, *96*, 062111.
32. Wang, X.; Ouyang, Y.; Li, X.; Wang, H.; Guo, J.; Dai, H. Room-Temperature All-Semiconducting Sub-10-nm Graphene Nanoribbon Field-Effect Transistors. *Phys. Rev. Lett.* **2008**, *100*, 206803.
33. Yazyev, O. V.; Katsnelson, M. I. Magnetic Correlations at Graphene Edges: Basis for Novel Spintronics Devices. *Phys. Rev. Lett.* **2008**, *100*, 047209.
34. Li, X.; Wang, X.; Zhang, L.; Lee, S.; Dai, H. Chemically Derived, Ultrasmooth Graphene Nanoribbon Semiconductors. *Science* **2008**, *319*, 1229–1232.